RSC Chemical Biology

ROYAL SOCIETY OF CHEMISTRY

PAPER

View Article Online
View Journal | View Issue

Cite this: *RSC Chem. Biol.*, 2025, **6**, 1414

Signals from the sea: the structural peculiarity of lipid A and weak immunostimulatory lipopolysaccharide from *Rheinheimera japonica*†

Stefania De Chiara,‡[a] Francesca Olmeo,‡[a] Emanuela Andretta,[ab] Luca De Simone Carone,[abc] Marcello Mercogliano,[a] Vlada S. Belova,[de] Lyudmila A. Romanenko,[d] Maxim S. Kokoulin,[d] Alba Silipo,[ab] Antonio Molinaro[ab] and Flaviana Di Lorenzo *[ab]

Lipopolysaccharides (LPSs) isolated from marine bacteria represent a valuable resource for biomedical innovation. Here, we report the first structural elucidation of the lipid A moiety and a preliminary immunological assessment of the full LPS from the marine Gram-negative *Rheinheimera japonica* KMM 9513^T. Using MALDI-TOF mass spectrometry (MS) and tandem MS, we show that the lipid A from *R. japonica* KMM 9513^T exhibits a heterogeneous architecture, composed of *mono*- and *bis*-phosphorylated tetra- and penta-acylated species with variations in the acyl chain length, saturation, branching, and positional isomerism. Functionally, the full LPS was found to be immunologically silent toward TLR4-mediated NF-κB activation in HEK-Blue™ hTLR4 cells and triggered only modest, dose-dependent responses in differentiated human THP-1 macrophages. Strikingly, the *R. japonica* LPS was able to antagonize *E. coli* LPS-induced TLR4 activation, even at low doses. Overall, this study uncovers a structurally and functionally atypical marine LPS with a dual profile, inactive towards TLR4 yet capable of modulating LPS-induced signaling. These findings offer a promising basis to consider *R. japonica* LPS as a source of structural inspiration for the design of synthetic derivatives with controlled immunological properties.

Received 29th May 2025,
Accepted 7th July 2025

DOI: 10.1039/d5cb00134j

rsc.li/rsc-chembio

Introduction

Rheinheimera japonica KMM 9513^T is a novel marine Gram-negative bacterium isolated from a sediment sample collected from the Sea of Japan seashore.[1] It has recently garnered interest due to its capability to produce low-molecular-weight metabolites with antibacterial activity.[1] Indeed, these antibacterial compounds, which are likely necessary for competition within microbial communities colonizing seashore sediments, have tremendous biotechnological and biomedical potential in controlling the growth of Gram-positive microorganisms in mariculture.[1] However, this discovery is not surprising as marine bacteria are an acknowledged source of novel bioactive compounds with a vast array of sustainable biotechnological applications across industries, spanning the range from pharmaceutical to environmental management.[2] To survive and proliferate in highly mutable and sometimes inhospitable habitats, in fact, they have evolved unique metabolic pathways and produce a variety of secondary metabolites that are not found in terrestrial bacteria. Likewise, marine bacteria often display specialized membrane structures that enable them to deal with the unique challenges of the aquatic environments.[3,4] Consequently, like their metabolites, membranes of marine bacteria exhibit several exceptional features not found in their terrestrial counterparts.

Like other Gram-negative bacteria, *R. japonica* displays an outer membrane that is characterized by the presence of lipopolysaccharides (LPSs), structural components that are key for maintaining membrane integrity and mediating interactions with external environments.[5,6] In marine habitats, in fact, an LPS not only acts as a shield but also plays a role in

[a] *Department of Chemical Sciences, University of Naples Federico II, via Cinthia, 4, 80126 Naples, Italy. E-mail: flaviana.dilorenzo@unina.it*
[b] *CEINGE-Biotecnologie Avanzate Franco Salvatore s.c.ar.l., Via G. Salvatore, 436, 80131 Naples, Italy*
[c] *Department of Biology, University of Naples Federico II, via Cinthia, 4, 80126 Naples, Italy*
[d] *G.B. Elyakov Pacific Institute of Bioorganic Chemistry, Far Eastern Branch, Russian Academy of Sciences, 159/2, Prospect 100 Let Vladivostoku, 690022 Vladivostok, Russia*
[e] *Far Eastern Federal University, 10 Ajax Bay, Russky Island, Vladivostok, 690922, Russia*

† Electronic supplementary information (ESI) available. See DOI: https://doi.org/10.1039/d5cb00134j

‡ These authors equally contributed to this work.

bacterial adhesion, biofilm formation, and interactions with other marine organisms. In general, an LPS, in its smooth form (S-LPS), is built up of three components, *i.e.* a glycolipid anchor to the membrane (lipid A), a rather short oligosaccharide (core OS), and a polysaccharide chain (O-antigen).[5,7] Depending on its chemical structure, an LPS can modulate host immune responses when marine bacteria encounter marine animals or, in rare cases, humans.[6] Therefore, studying the structural and immunological characteristics of marine bacterial LPS can provide insights into the environmental adaptations of these microorganisms and their potential impact on human and animal health. However, despite the increasing interest in the genus *Rheinheimera*, very little is known about the chemistry of its LPSs, their role in the bacterium environmental adaptability and the possible interactions with and/or impact on the human innate immune system. As a matter of fact, an LPS, and in particular its lipid A moiety, is recognized by the human innate immune system *via* the receptor complex made up of toll-like receptor 4 (TLR4) and myeloid differentiation protein-2 (MD-2), which is present on the surface of, among others, macrophages, neutrophils, and dendritic cells.[5] The recognition of LPS by TLR4/MD-2 triggers a signaling cascade that ultimately leads to the production of pro-inflammatory cytokines, which aids in the clearance of invading pathogens.[8] On the other hand, overproduction of these inflammatory mediators can result in severe pathological outcomes, such as septic shock, chronic inflammatory diseases, and even cancer. In this frame, the search for antagonists/inhibitors is a critical area of research focused on developing therapies to control this excessive inflammation driven by TLR4 signaling.[9,10] In this frame, marine bacteria are seen as a promising source of LPS molecules with TLR4 inhibitory properties. Indeed, unlike terrestrial LPSs, marine LPSs often exhibit structural characteristics that result in altered immune responses, including different profiles of TLR4 activation or inhibition.[6]

Within this frame, we elucidated the structure of the *R. japonica* KMM 9513^T lipid A moiety obtained by merging data from chemical analyses and making use of matrix-assisted laser desorption/ionization-time of flight mass spectrometry (MALDI-TOF MS) and tandem MS (MS/MS). In parallel, we also investigated *in vitro* the immunological properties of its purified LPS and discovered that it was unable to activate a TLR4 response, while it antagonized NF-κB activation triggered by a toxic LPS. These functional properties are tempting to leave some space for *R. japonica* KMM 9513^T LPSs in future anti-sepsis therapies by dampening overactive immune responses.

Results

Isolation of LPS from *R. japonica* KMM 9513^T and compositional analyses of lipid A

LPS was isolated from dried *R. japonica* KMM 9513^T cells using the hot phenol/water extraction method, which was followed by thorough purification involving enzymatic digestion, dialysis, ultracentrifugation, and size-exclusion chromatography.

Table 1 Fatty acid content of lipid A from *R. japonica* KMM 9513^T. 3-Hydroxy fatty acids displayed an (*R*) configuration. The position of the double bond and the stereochemistry of the unsaturated fatty acids remain to be identified. The stereochemistry of *anteiso*-branched acyl chains is tentatively given as *S*, found principally in bacteria; however, it remains to be confirmed

Fatty acid content	
10:0	*a*14:0
*i*12:0	14:0
12:0	*i*15:0
*i*13:0	*a*15:0
*a*13:0	15:0
13:0	16:1
12:0(3-OH)	*i*16:0
14:1(3-OH)	*i*17:0
*i*14:0	*a*17:0

Additionally, to get rid of any possible lipoprotein/lipopeptide contamination, a repurification step was also performed. To assess the purity and nature of the isolated material, SDS-PAGE followed by silver nitrate gel staining revealed a band at high molecular weight indicating the presence of a smooth-type LPS (S-LPS), which was consistent with our previous analysis.[11] To obtain structural information of lipid A, an aliquot of LPS was subjected to mild acid hydrolysis and subsequent centrifugation to selectively cleave the linkage between the first sugar of the core OS, *i.e.* 3-deoxy-D-*manno*-octulosonic acid (Kdo), and the non-reducing glucosamine of the lipid A portion. An aliquot of isolated lipid A was subjected to methanolysis followed by acetylation to analyze the fatty acids as methyl esters and to identify the sugar components of the lipid A backbone. The analysis revealed a heterogeneous fatty acid composition (Table 1) characterized by a high abundance of 12:0(3-OH) and 12:0, with the latter found both in linear and branched forms. Additionally, the lipid A backbone was found to be composed exclusively of 2-amino-2-deoxy-D-glucose (D-glucosamine), as expected.

MALDI-TOF MS and MS/MS of lipid A from *R. japonica* KMM 9513^T

Another aliquot of lipid A, obtained *via* mild acid hydrolysis of LPS, was observed *via* a detailed MALDI-TOF MS and MS/MS analysis. The MALDI-TOF MS spectrum of lipid A from *R. japonica* KMM 9513^T was recorded in resolution mode with negative-ion polarity (Fig. 1). The spectrum clearly showed the presence of two main clusters of peaks at around *m*/*z* 1301.76 and *m*/*z* 1499.92, corresponding to $[M–H]^-$ ions of *bis*-phosphorylated tetra- and penta-acylated lipid A species, respectively (Table 2). Less intense peaks were detected at around *m*/*z* 1221.79 and *m*/*z* 1419.96, which were attributed to their *mono*-phosphorylated counterparts. The complexity observed within each cluster, which was reflected by the presence of peaks differing by 14 amu (–CH_2– units) and 2 amu, suggested structural microheterogeneity due to variations in the acyl chain length and the degree of their unsaturation, in agreement with compositional analysis (Table 1). In detail, the most intense peaks within each cluster, *i.e.* at *m*/*z* 1301.75 and *m*/*z* 1499.92, were assigned to *bis*-phosphorylated tetra- and

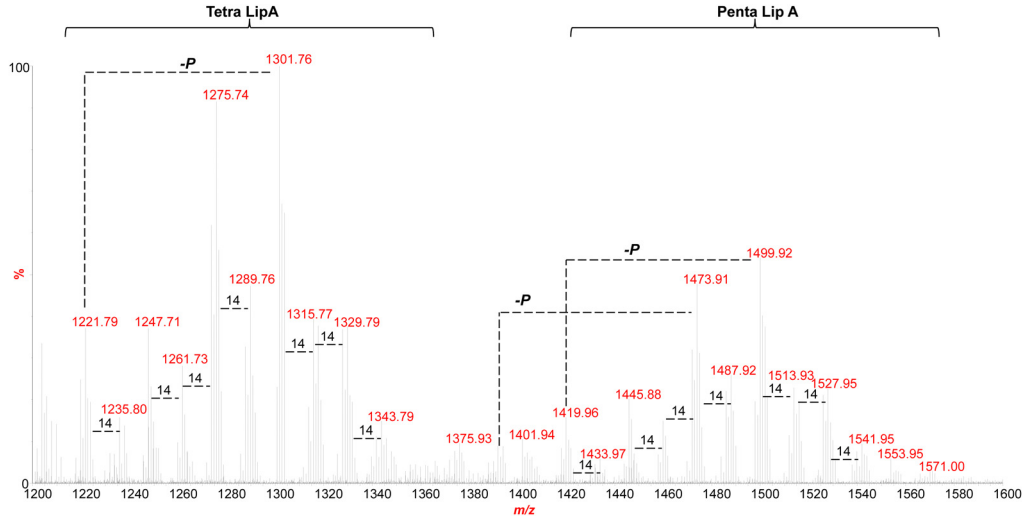

Fig. 1 High-resolution, negative-ion MALDI-TOF MS spectrum of lipid A from *R. japonica* KMM 9513^T. The two main clusters of peaks are associated with *bis*-phosphorylated tetra-acylated and penta-acylated lipid A species labelled as Tetra LipA and Penta LipA, respectively. The spectrum also reveals the presence of their respective *mono*-phosphorylated forms. "*−P*" indicates the lack of a phosphate group.

Table 2 The main ion peaks observed in the MALDI-TOF MS spectrum (Fig. 1) are listed along with their corresponding theoretical monoisotopic masses and structural assignments. Each experimental *m/z* value is compared to the calculated exact mass derived from the proposed lipid A structures

Predicted mass (Da)	Observed ion peaks (*m/z*)	Acyl substitution	Proposed composition
1500.91	1499.93	Penta-acyl	HexN^2, P^2, [12:0(3-OH)]^3 (12:0) [14:1(3-OH)]
1514.93	1513.93	Penta-acyl	HexN^2, P^2, [12:0(3-OH)]^3 (13:0) [14:1(3-OH)]
1474.89	1473.91	Penta-acyl	HexN^2, P^2, [12:0(3-OH)]^4 (12:0)
1302.75	1301.76	Tetra-acyl	HexN^2, P^2, [12:0(3-OH)]^2 (12:0) [14:1(3-OH)]
1276.73	1275.75	Tetra-acyl	HexN^2, P^2, [12:0(3-OH)]^3 (12:0)
1248.70	1247.76	Tetra-acyl	HexN^2, P^2, [12:0(3-OH)]^3 (10:0)
1222.78	1221.78	Tetra-acyl	HexN^2, P, [12:0(3-OH)]^2 (12:0) [14:1(3-OH)]

penta-acylated lipid A species composed of two glucosamine units bearing one 12:0 (*iso*12:0 or *anteiso*12:0), one 14:1(3-OH), and either two or three 12:0(3-OH) residues, respectively. For simplicity hereafter, acyl chains are described without specifying branching, although *iso* and *anteiso* forms were detected *via* compositional analysis (Table 1). Notably, besides the variations in the acyl chain length and number, prominent peaks at *m/z* 1275.74 and *m/z* 1473.91, that is, 26 amu lower than the aforementioned species, revealed an additional layer of heterogeneity, attributable to the presence of shorter and/or unsaturated acyl chains. To elucidate the structural details of this lipid A mixture, a detailed negative-ion MS/MS investigation was conducted. The MS/MS spectrum of the precursor ion at *m/z* 1499.92 (Fig. 2A) displayed intense peaks at *m/z* 1401.94 originated from the loss of a phosphate group, and at *m/z* 1284.10 and *m/z* 1186.10 produced *via* the loss of a 12:0(3-OH) and the sequential loss of a phosphate and 12:0(3-OH), respectively. A lower-intensity peak corresponding to the loss of one phosphate and two 12:0(3-OH) was also observed at *m/z* 969.87, whereas the peak at *m/z* 769.63 reflected further loss of a 12:0. The detection of the Y_1 ion[12] at *m/z* 654.56, resulting from the cleavage of the glycosidic bond of the glucosamine disaccharide backbone, enabled the location of two 12:0(3-OH) on the reducing glucosamine unit. This structural hypothesis was reinforced by the observation of the peak at *m/z* 904.81 originated from the $^{0,4}A_2$ cross-ring fragmentation,[12] which in turn allowed placing one 12:0(3-OH), one 14:1(3-OH) and the 12:0 on the non-reducing glucosamine. In support, related $^{0,4}A_2$ fragments lacking one 12:0(3-OH) or both one 12:0(3-OH) and the 12:0 were also observed at *m/z* 706.60 and *m/z* 506.36, respectively. Together, these data confirmed the nature of the primary acyl chains decorating the non-reducing glucosamine, *i.e.* an *O*-linked 12:0(3-OH) and an *N*-linked 14:1(3-OH), with the latter in turn carrying the secondary 12:0. The absence of peaks corresponding to the simple loss of 14:1(3-OH) or a full 12:0-bearing hydroxylated acyl chain further corroborated this structural assignment. Negative-ion MS/MS analysis of precursor ions at *m/z* 1513.93 (Fig. S1A, ESI†) and *m/z* 1473.91 (Fig. 2B), which were also attributed to *bis*-phosphorylated penta-acylated lipid A species, uncovered additional structural heterogeneity (Table 2). In particular, the structure deduced for the species at *m/z* 1473.91 was similar to that for the species at *m/z* 1499.92, but with a 12:0(3-OH) replacing the unsaturated 14:1(3-OH) (Fig. 2B).

This hypothesis was confirmed by the presence, among others, of the Y_1 ion at *m/z* 654.55 and the cross-ring

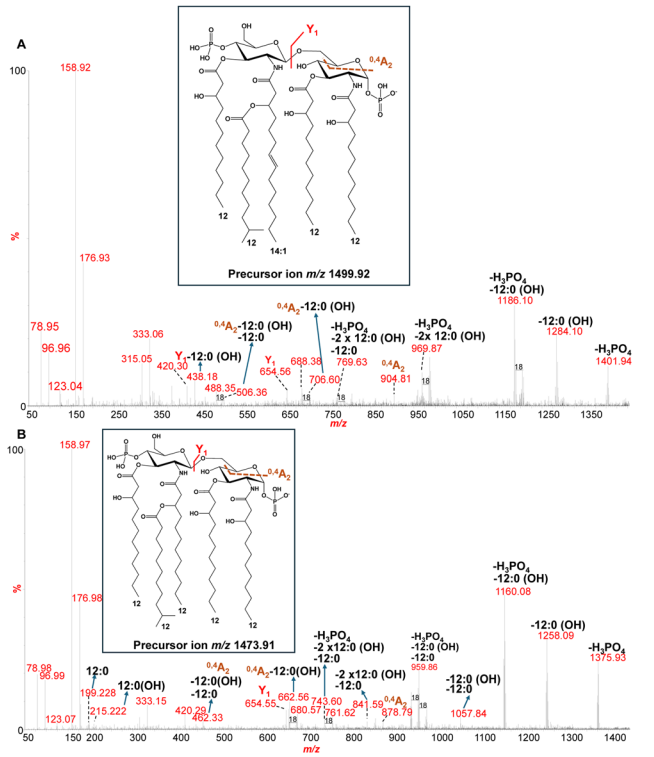

Fig. 2 Negative-ion high-resolution MALDI-TOF MS/MS spectrum of *bis*-phosphorylated penta-acylated lipid A species at *m/z* 1499.92 (A) and *m/z* 1473.91 (B). The assignment of major fragments is shown in both spectra, and the proposed structures are shown as insets. Acyl chains are represented with 12:0 in its iso form for illustrative purposes only; the actual composition may include linear and anteiso forms as well.

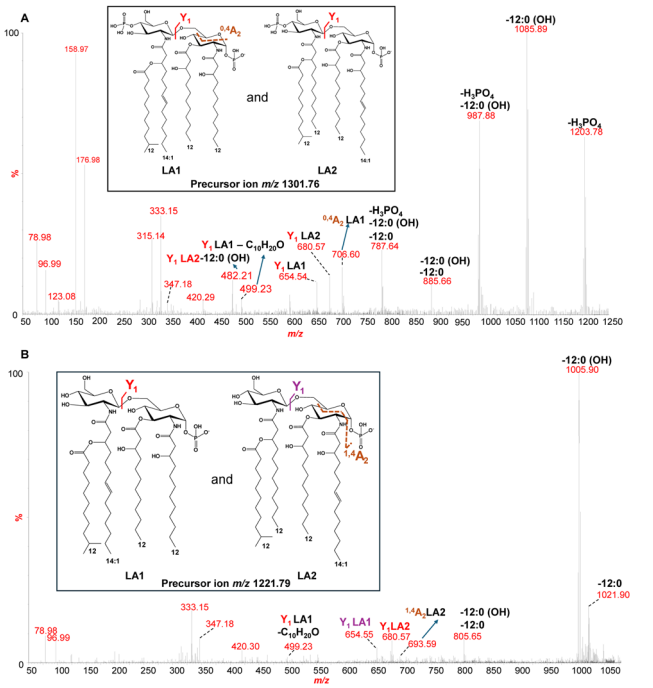

Fig. 3 Negative-ion high-resolution MALDI-TOF MS/MS spectrum of tetra-acylated lipid A species at *m/z* 1301.76 (A) and *m/z* 1221.79 (B). The assignment of major fragments is reported, and the proposed structures are sketched in each inset. Acyl chains are denoted with 12:0 in its iso form for description purposes only; the actual composition may include linear and anteiso forms as well.

fragmentation $^{0,4}A_2$ at *m/z* 878.79. Analysis of the MS/MS spectrum of the precursor ion at *m/z* 1275.75 (Fig. S1B, ESI†) guided the assignment of this species to tetra-acylated lipid A structurally analogous to the one at *m/z* 1473.91 but lacking the primary *O*-linked 12:0(3-OH) on the non-reducing glucosamine. Indeed, fragment ions at *m/z* 1177.76, *m/z* 1059.55, and *m/z* 977.58 were consistent with the loss of a phosphate, a 12:0(3-OH), and both, respectively. Additional fragments at *m/z* 859.38 and 761.40 indicated sequential losses of 12:0 and 12:0(3-OH), with or without phosphate. The Y_1 ion at *m/z* 654.36 supported the placement of two 12:0(3-OH) on the reducing glucosamine and, therefore, of one 12:0(3-OH) and one 12:0 on the non-reducing one. Interestingly, the peak at *m/z* 1513.93 (Fig. S1A, ESI†), which might initially appear to be an acyl chain length variant of the species detected at *m/z* 1499.93 (*i.e.* plus an additional –CH_2– unit), actually corresponded to a structurally distinct molecule, in which the 12:0 is replaced by a 13:0, and the positions of the 12:0(3-OH) and 14:1(3-OH) chains are inverted, thus placing the unsaturated acyl chain on the reducing glucosamine (Fig. S1A, ESI†). The structural assignment was primarily guided by the detection of the Y_1 ion at *m/z* 680.54, alongside other characteristic lipid A fragments. These included ions at *m/z* 983.80, resulting from the loss of two 12:0(3-OH) and one phosphate group, and at *m/z* 985.87, corresponding to the sequential loss of a 12:0(3-OH) and the 13:0 unit.

A similar approach was applied to the analysis of precursor ions at *m/z* 1301.76 and *m/z* 1221.79, corresponding to tetra-acylated lipid A species (Fig. 3). This investigation revealed additional structural heterogeneity in the lipid A of *R. japonica* KMM 9513^T, which was not due to differences in the fatty acid composition, but rather to the positional distribution of the amide-linked primary acyl chains. Specifically, two isobaric lipid A species (LA1–LA2, Fig. 3 and 4) were identified. In one species, the reducing glucosamine is substituted with two 12:0(3-OH), while the non-reducing one carries a 14:1(3-OH) and the secondary 12:0 (LA1); in the other species (LA2), this arrangement is reversed for the sole amide-bound fatty acids. Briefly, main peaks at *m/z* 1204.11, *m/z* 1085.89 and *m/z* 987.88 reflected losses of phosphate, 12:0(3-OH), and both, respectively. However, Y_1 ions at *m/z* 654.54 and *m/z* 680.57 provided diagnostic evidence for the presence either of two 12:0(3-OH) (*m/z* 654.54) or one 12:0(3-OH) and one 14:1(3-OH) (*m/z* 680.57) on the reducing glucosamine. Fragments originated from the loss of 156 amu ($C_{10}H_{20}O$) were also observed. These were ascribed to an enamine–imine tautomerization followed by a six-membered ring rearrangement, a process that can only occur when the *N*-linked acyl chains, such as 12:0(3-OH) in this case, do not carry secondary acyl substituents. Therefore, their observation concurred to place acyl moieties on the disaccharide backbone.[13] Analogously, the analysis of the *mono*-phosphorylated species at *m/z* 1221.79 (Fig. 3B) confirmed the same structural heterogeneity and enabled the

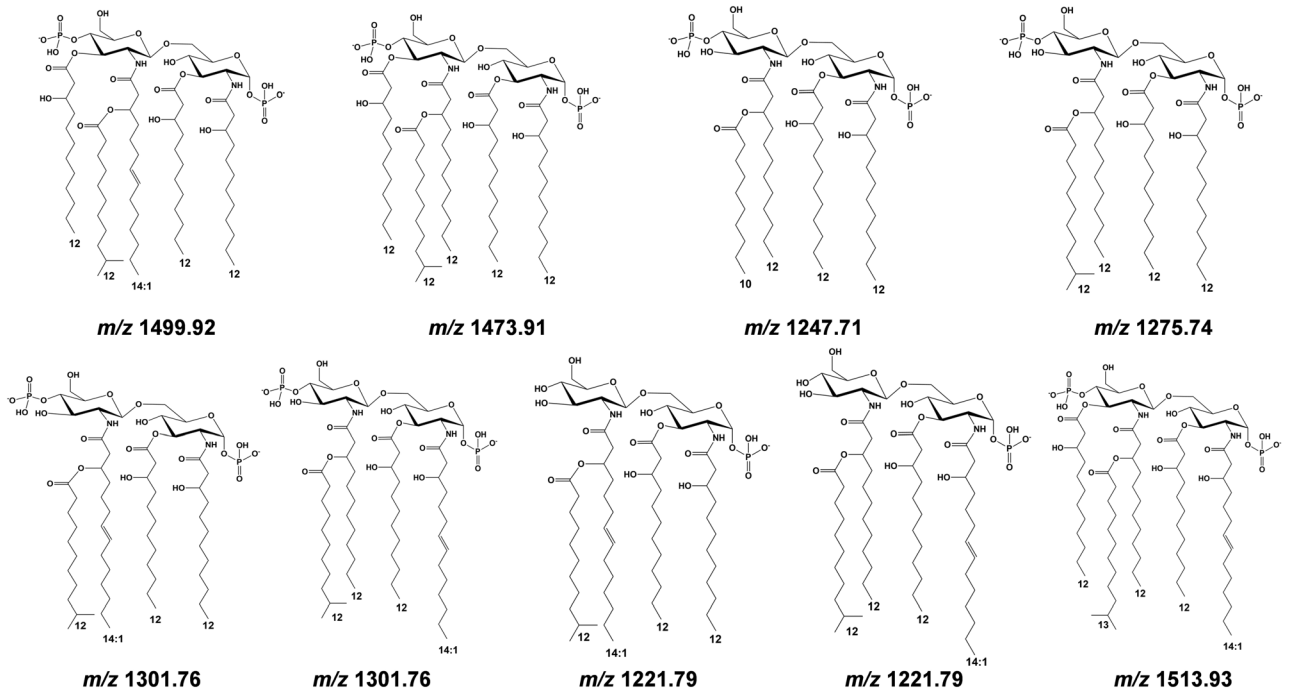

Fig. 4 Proposed structures for lipid A species of *R. japonica* KMM 9513^T deduced from the interpretation of MALDI-TOF MS and MS/MS analyses and compositional analyses (see also Table 2).

placement of the phosphate group on the reducing glucosamine, as demonstrated by the corresponding Y_1 and $^{1,4}A_2$ cross-ring fragment ions at *m*/*z* 654.55 (Y_1 LA1), 680.57 (Y_1 LA2), and 693.59 ($^{1,4}A_2$ LA2).

In conclusion, by combining compositional data with in-depth MS and MS/MS analysis, we observed an unexpected degree of structural heterogeneity in the lipid A of *R. japonica* KMM 9513^T, driven by variations in the acyl chain composition, number and positional isomerism (Fig. 4).

Immunological effects of the *R. japonica* KMM 9513^T LPS on HEK cells

The structural microheterogeneity uncovered in the lipid A of *R. japonica* KMM 9513^T prompted us to explore its immunological properties. Variations in the number, type, and position of acyl chains, as well as in the number and location of the phosphates, critically influence the recognition of LPS by the host immune system, particularly through the TLR4/MD-2 receptor complex.[5,8] Therefore, we sought to determine whether the structural complexity observed in *R. japonica* KMM 9513^T lipid A is reflected in a peculiar immunostimulatory behavior, with an emphasis on TLR4-dependent signaling. Therefore, we employed HEK-Blue™ hTLR4 cells stably transfected with TLR4, MD-2, and CD14 genes and engineered these with a SEAP reporter gene under the control of an NF-κB/AP-1-inducible promoter to assess TLR4-mediated NF-κB activation in response to LPS stimulation. We used increasing concentrations (1, 10, and 100 ng mL^{-1}) of *R. japonica* KMM 9513^T LPS and *E. coli* LPS, with the latter used as a positive control for pro-inflammatory activation. As shown in Fig. 5A, *R. japonica* KMM 9513^T LPS induced markedly lower NF-κB activity compared to *E. coli* LPS across all tested concentrations. Notably, NF-κB activation in *R. japonica* LPS-treated cells was indistinguishable from that observed in unstimulated controls, indicating a lack of detectable TLR4-mediated signaling. Given that certain atypical LPS structures are known to activate TLR2, we investigated whether *R. japonica* LPS could elicit a response through this alternative pathway. HEK-Blue™ hTLR2 cells, which stably express human TLR2, were stimulated with increasing concentrations of *R. japonica* LPS, while PAM3CSK4 was used as a positive control. As shown in Fig. 5B, *R. japonica* LPS failed to induce any detectable TLR2-mediated NF-κB activation, with responses comparable to those of unstimulated cells. Then, we moved to evaluating whether the *R. japonica* LPS, like LPSs from other marine bacteria, was able to antagonize TLR4 signaling by interfering with the activation induced by a pro-inflammatory LPS, like *E. coli* LPS. To this aim, HEK-Blue™ hTLR4 cells were pre-treated for 4 hours with *R. japonica* LPS or with the *Rhodobacter sphaeroides* (RS) LPS (0.1, 1, 10, and 100 ng mL^{-1}), a well-characterized TLR4 antagonist. After pre-incubation, cells were stimulated with either 10 or 100 ng mL^{-1} of *E. coli* LPS for 16 hours, and NF-κB activation was then quantified. As shown in Fig. 5C and D, pre-treatment with RS LPS significantly reduced *E. coli* LPS-induced NF-κB activation as expected, thus confirming its antagonistic activity. Strikingly, pre-treatment with *R. japonica* LPS substantially reduced the response to 10 ng mL^{-1} *E. coli* LPS, and this antagonistic effect was maintained even under high-dose stimulation (100 ng mL^{-1} *E. coli* LPS), thus showing a clear inhibitory effect on TLR4 activation. Notably, at 1 ng mL^{-1},

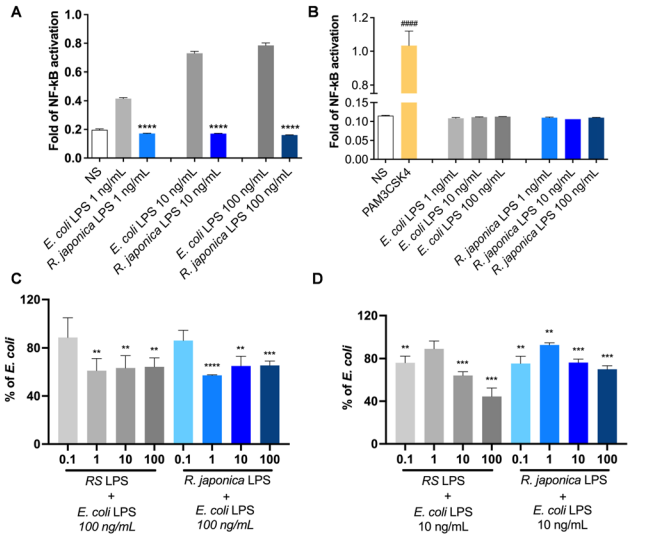

Fig. 5 Stimulation of HEK-Blue™ hTLR4 (A) and HEK-Blue™ hTLR2 (B) cells. SEAP levels (OD 620 nm) following stimulation with 1, 10, and 100 ng mL^{-1} of *E. coli* O111:B4 LPS (*E. coli* LPS) or *R. japonica* KMM 9513^T (*R. japonica*) LPS were evaluated using the Quanti-Blue assay. Data are shown as mean ± standard deviation. Significant differences between *R. japonica* LPS and *E. coli* LPS (****p-value <0.0001) and between PAM3CSK4 and NS ($^{\#\#\#}p$-value <0.001) were evaluated *via* Student's *t* test. (C) and (D) Competition assays between *R. japonica* LPS and *E. coli* LPS for human TLR4. Fold of NF-kB activation in HEK Blue hTLR4 cells primed with the potent TLR4 antagonist *Rhodobacter sphaeroides* (RS) or *R. japonica* LPS (0.1–1–10–100 ng mL^{-1}) for 4 hours and then stimulated with 100 ng mL^{-1} (C) or 10 ng mL^{-1} (D) of *E. coli* LPS for 16 hours. Data are expressed as a percentage *versus* 10 ng mL^{-1} or 100 ng mL^{-1} *E. coli* LPS values considered as 100% and shown as mean ± standard deviation. Significant differences between *R. japonica* or *RS* LPS and *E. coli* LPS (**p-value <0.01; ***p-value <0.001; ****p-value <0.0001 *vs E. coli* LPS) were evaluated *via* Student's *t* test.

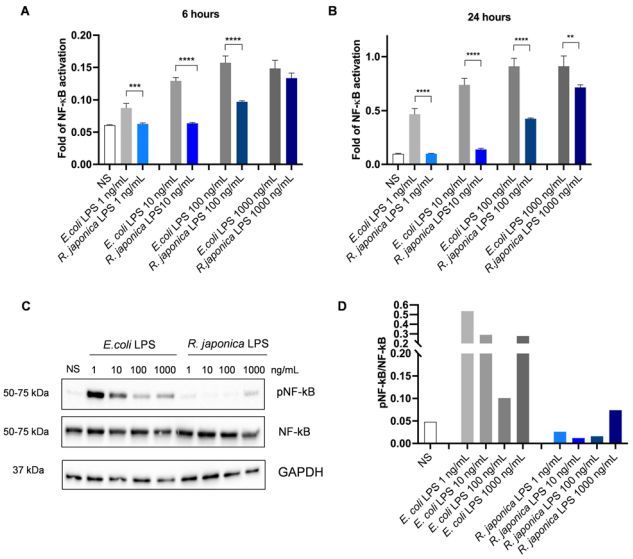

Fig. 6 Stimulation of PMA-differentiated THP1-Blue™ NF-κB cells. NF-kB-dependent SEAP levels (OD 620 nm) following 6- (A) and 24-hour (B) stimulation with 1, 10, 100, and 1000 ng mL^{-1} of *E. coli* O111:B4 LPS (*E. coli* LPS) or *R. japonica* LPS were evaluated using the Quanti-Blue assay. Unstimulated cells (NS) are the negative control. Data are shown as mean ± standard deviation. Significant differences between *R. japonica* LPS and *E. coli* LPS (**p-value <0.01; ***p-value <0.001; ****p-value <0.0001 *vs. E. coli* LPS) were evaluated using Student's *t* test. (C and D) Effect of *R. japonica* LPS on phospho and total NF-kB protein levels in PMA-differentiated THP1 cells. Levels of total and phosphorylated NF-kB were evaluated by western blotting on cells stimulated with *E. coli* O111:B4 (*E. coli*) or *R. japonica* LPS for 24 hours. (C) Representative images of phospho NF-kB, total NF-kB and GAPDH are shown. (D) Densitometric analysis of the phospho NF-kB/total NF-kB ratio.

R. japonica LPS was able to reduce the NF-κB response to 100 ng mL^{-1} *E. coli* LPS by approximately 40% (Fig. 5C), demonstrating an inhibitory capacity comparable to that of RS LPS.

Immunological effects of the *R. japonica* KMM 9513^T LPS on human macrophages

To further explore the immunological properties of the *R. japonica* KMM 9513^T LPS, we extended our analysis to THP1-Blue™ NF-κB cells, a human monocytic cell line commonly used as a model for macrophage responses.[14,15] Since undifferentiated THP-1 cells are poorly responsive to LPS stimulation, cells were first differentiated into a macrophage-like phenotype using PMA treatment.[16] As an initial step, we assessed whether the *R. japonica* KMM 9513^T LPS exerted any cytotoxic effect on these cells. Differentiated THP-1 cells were stimulated for 24 hours with increasing concentrations of either *R. japonica* or *E. coli* LPS, and cell viability was evaluated in comparison to unstimulated controls. As expected, the *E. coli* LPS significantly reduced THP-1 cell viability, whereas the *R. japonica* LPS had no significant impact, even at the highest concentrations tested (Fig. S2A, ESI†). Next, we assessed the ability of the *R. japonica* KMM 9513^T LPS to activate NF-κB signaling in differentiated THP-1 cells. Cells were treated for 6 or 24 hours with either *R. japonica* LPS or *E. coli* LPS (1, 10, 100, and 1000 ng mL^{-1}), while unstimulated cells were used as a negative control. The highest dose (1000 ng mL^{-1}) was included in these experiments to determine whether stronger stimulation could trigger potent NF-κB activation. As shown in Fig. 6A and B, the *R. japonica* KMM 9513^T LPS induced, in a dose-dependent manner, a significantly lower NF-κB activation compared to *E. coli* LPS at all tested concentrations and time points, thus confirming the trend observed in HEK-Blue hTLR4 cells (Fig. 5A). At the highest concentrations tested (100 and 1000 ng mL^{-1}), the *R. japonica* KMM 9513^T LPS could elicit a higher NF-κB response, indicating a residual, though limited, immunostimulatory potential. These results were further corroborated by western blot analysis performed to quantify total NF-κB and its phosphorylated form (phospho-NF-κB) (Fig. 6C and D). As expected, stimulation with the *E. coli* LPS led to a pronounced increase in NF-κB phosphorylation compared to unstimulated cells. In contrast, the *R. japonica* LPS induced a weaker phosphorylation signal, consistent with an attenuated NF-κB activation profile. To investigate whether the NF-κB activation induced by the *R. japonica* KMM 9513^T LPS was TLR4-dependent in this cell line, we pre-treated differentiated THP-1 cells with a blocking anti-TLR4 antibody prior to

stimulation. As expected, pre-treatment completely abrogated the response to *E. coli* LPS, confirming effective inhibition of TLR4-mediated signaling (Fig. S2B, ESI†). However, stimulation with high concentrations of the *R. japonica* KMM 9513^T LPS ($\geq$100 ng mL^{-1}) still resulted in measurable NF-κB activation despite TLR4 blockade (Fig. S2B, ESI†). This remaining activation suggests the possible involvement of TLR4-independent pathways or partial engagement of alternative pattern recognition receptors that become relevant only at elevated LPS concentrations.

We then measured the secretion of pro-inflammatory IL-8, IL-6, and TNF-α in differentiated THP-1 cells following 24-hour stimulation with increasing concentrations of *R. japonica* KMM 9513^T or *E. coli* LPS. As expected, the *E. coli* LPS triggered a robust IL-8 release, whereas the *R. japonica* KMM 9513^T LPS induced significantly lower IL-8 production at all tested doses (1–100 ng mL^{-1}) and was almost undetectable in cells treated with 1 or 10 ng mL^{-1} of *R. japonica* LPS (Fig. 7A). A similar trend was observed for IL-6, *i.e.* while *E. coli* LPS induced its release (at 10 and 100 ng mL^{-1}), IL-6 remained below the detection limit in cells treated with *R. japonica* LPS (Fig. 7B). TNF-α production was investigated at both 6 and 24 hours post-stimulation, as this cytokine is known to be an early marker of LPS-induced inflammation with rapid kinetics and a short half-life in cell culture systems. As expected, stimulation with *E. coli* LPS induced higher TNF-α levels at 6 hours than at 24 hours (Fig. 7C). In contrast, *R. japonica* LPS at 10 ng mL^{-1} failed to elicit detectable TNF-α secretion at either time points (Fig. 7C). However, stimulation with 100 ng mL^{-1} of *R. japonica*

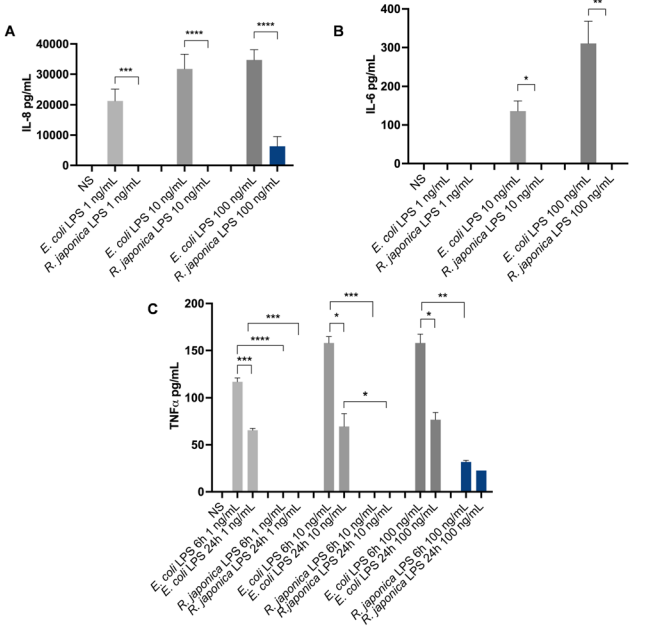

Fig. 7 Cytokine release following *R. japonica* LPS stimulation of PMA-differentiated THP1 cells. The levels of IL-8 (A), IL-6 (B) and TNF-α (C) (pg mL^{-1}) in cell supernatants were assessed *via* ELISA. Data are shown as mean ± standard deviation. Significant differences between *R. japonica* LPS and *E. coli* LPS (*p-value <0.05; **p-value <0.01; ***p-value <0.001 *vs. E. coli* LPS) were evaluated using Student's *t* test.

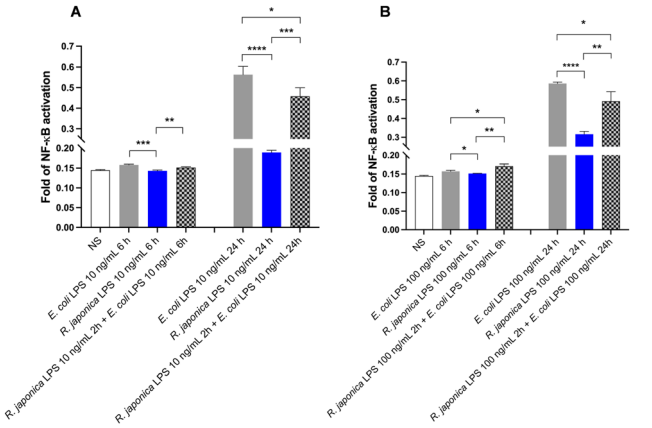

Fig. 8 Competition assay between *R. japonica* LPS and *E. coli* LPS on PMA-differentiated THP1. Fold of NF-kB activation in cells primed with *R. japonica* LPS at 10 (A) and 100 ng mL^{-1} (B) for 2 hours and then, once removed, stimulated with 10 ng mL^{-1} or 100 ng mL^{-1} of *E. coli* LPS for 6 and 24 hours. Significant differences (*p-value <0.05; **p-value <0.01; ***p-value <0.001; ****p-value <0.0001) were evaluated using Student's *t* test.

KMM 9513^T LPS resulted in low, yet measurable, TNF-α production. This further suggested that *R. japonica* LPS leads to a dramatically weaker and more transient inflammatory response in THP-1 cells.

Finally, to assess the ability of *R. japonica* KMM 9513^T LPS to modulate *E. coli* LPS-induced NF-κB activation in THP-1 cells, we employed two experimental setups. At first, as previously performed with HEK-Blue™ hTLR4 cells, THP-1 cells were pre-treated for 4 hours with *R. japonica* LPS, and the LPS was maintained in the culture medium during the subsequent stimulation with *E. coli* LPS for 24 hours (Fig. S2C and D, ESI†). In the second approach, cells were pre-treated with *R. japonica* LPS at 10 or 100 ng mL^{-1} for only 2 hours, followed by thorough washing to remove the LPS, and then stimulated with *E. coli* LPS for an additional 6 or 24 hours. As shown in Fig. 8, even the shorter pre-treatment with *R. japonica* LPS, despite its removal prior to *E. coli* LPS exposure, was sufficient to significantly reduce NF-κB activation for at least 24 hours, indicating that transient exposure can trigger a long-lasting inhibitory effect. Likewise, in the 4-hour pre-treatment condition (Fig. S2C and D, ESI†) where *R. japonica* LPS was present during *E. coli* LPS stimulation, a strong suppression of NF-κB activation was also observed in accordance with the results on HEK-Blue™ hTLR4 cells.

Discussion

The marine environment forces unique selective pressures on microbial populations, boosting structural adaptations that improve membrane stability and flexibility, both essential to guaranteeing bacterial survival and proliferation in dynamic marine habitats.[17] In this context, the outer membrane architecture of Gram-negative marine bacteria, and particularly the structure of their lipid A, plays a crucial role in coping with

salinity, temperature, and hydrostatic pressure fluctuations. The lipid A of *R. japonica* KMM 9513^T is a clear illustration of this adaptability, as it presents a structurally heterogenous profile that may contribute to environmental resilience and ecological competitiveness. By leveraging chemical analyses, MALDI-TOF MS and MS/MS, we showed that the lipid A moiety from *R. japonica* KMM 9513^T consists of a complex mixture of *mono* and *bis*-phosphorylated tetra- and penta-acylated species, varying in acyl chain number, length, degree of saturation, and branching. These species predominantly carry 12:0(3-OH) and/or the uncommon 14:1(3-OH) as primary acyl chains. Notably, we observed isobaric species differing in the positioning of acyl chains on the glucosamine backbone, highlighting an additional layer of structural microheterogeneity. Therefore, unlike canonical and extensively studied lipid A moieties from Enterobacteria, lipid A from *R. japonica* KMM 9513^T features a remarkable level of structural complexity, not only in the fatty acid chain composition, but critically in the positional isomerism of acyl substitutions. While such complexity is not uncommon among marine bacteria,[18–22] their precise configuration might support a membrane architecture that likely enhances fluidity and resistance to environmental perturbation, which are properties that are pivotal and advantageous in marine ecosystems. For instance, the coexistence of unsaturated acyl chains among the primary fatty acids indicates a finely tuned system to optimize bilayer fluidity.[23] The presence of unsaturated acyl chains, in fact, especially when positioned as primary substituents, can lower the phase transition temperature of the membrane, thus preserving flexibility where more rigid saturated lipids would otherwise hinder the membrane function.[23–25] Similarly, branched fatty acids are largely known to disturb tight lipid packing, which in turn enhances membrane flexibility and possibly modulates permeability.[23–25] In addition, our analyses also revealed positional isomerism of the N-linked primary acyl chains on the glucosamine disaccharide backbone. While such an acyl chain rearrangement is not unprecedented in Gram-negative bacteria,[26] its prominence in *R. japonica* supports the idea of a certain degree of enzymatic flexibility or plasticity in the biosynthetic machinery, possibly driven by environmental cues.

Beyond their structural and ecological relevance, marine LPSs that display uncommon structural features in their lipid A moieties typically exhibit equally unusual immunological properties.[6] In this regard, our *in vitro* experiments on the whole *R. japonica* KMM 9513^T LPS molecule uncovered an intriguing example of marine LPSs with potential biomedical implications. Despite expressing molecular features generally required for TLR4 activation (such as bis-phosphorylation and acyl chains of appropriate length, like C14 and C12),[27] the *R. japonica* LPS failed to trigger NF-κB signaling in HEK-Blue™ hTLR4 cells and only induced a weak, concentration-dependent response in human macrophage-like THP-1 cells. More remarkably, it consistently antagonized *E. coli* LPS-induced NF-kB activation exerting a persistent inhibitory signal even after its removal. These findings support the view that the *R. japonica* KMM 9513^T LPS functions as a stable and potent TLR4 antagonist capable of dampening inflammatory responses in the presence of a potent agonist. This behavior resembles that of other structurally atypical LPS molecules, such as those from *R. sphaeroides* or *Porphyromonas gingivalis*, which are weak TLR4 agonists and are known to induce limited and transient pro-inflammatory responses.[28,29] This immunological behavior is typically associated with hypoacylation (*i.e.* the presence of less than six acyl chains), hypophosphorylation and/or unusual fatty acid patterns,[30–32] features also observed in *R. japonica* KMM 9513^T lipid A, thus supporting the hypothesis that its structural microheterogeneity contributes to the attenuated immunostimulatory capacity. Interestingly, unlike *E. coli* LPS, which was fully neutralized by TLR4 blockade, *R. japonica* LPS triggered low but detectable NF-κB activation in THP-1 cells at high concentrations even in the presence of the anti-TLR4 antibody. This suggests the engagement of alternative signaling pathways independent of TLR4, potentially involving other receptors expressed in macrophage-like cells but absent in HEK-TLR4 models. In this frame, recent studies have pointed to a possible crosstalk between carbohydrate-binding proteins (lectins), LPSs and TLR4, showing that specific glycan structures, especially those exposing terminal or lateral residues, can influence innate immune responses.[7,33–36] As a matter of fact, the O-antigen of *R. japonica* KMM 9513^T has a peculiar composition that includes 2-acetamido-2-deoxy galactose (GalNAc), 4-acetamido-4,6-dideoxy hexose (Qui4NAc), and the acidic monosaccharide galacturonic acid (GalA).[11] However, this polysaccharide is overall neutral, as GalA occurs in the amide form and is glycosylated by Qui4NAc through an unusual *N*-glycosidic bond.[11] Therefore, it is tempting to hypothesize that the O-antigen, through its unique chemical features, could induce NF-kB activation indirectly by engaging lectins as co-receptors as observed for other LPSs.[35,37] For instance, at high concentrations, the GalNAc-containing O-antigen of *R. japonica* LPS might be recognized by macrophage galactose-type lectin, a C-type lectin receptor expressed in differentiated THP-1 cells[38] and known to bind GalNAc, which under certain conditions promotes NF-kB activation.[39] In addition, TLR4-independent pathways may also play a role, possibly involving intracellular sensing or alternative pattern recognition receptors.[7] This possibility merits further investigation and may be of particular interest to those exploring LPS recognition systems beyond the canonical TLR4 axis.

Overall, our findings underscore the TLR4-silent yet immunomodulatory nature of the *R. japonica* KMM 9513^T LPS, distinguishing it from conventional pro-inflammatory LPSs. This is particularly relevant given the increasing interest in identifying natural LPS variants that can modulate immune response.[40–42] Indeed, with its attenuated pro-inflammatory activity and effective TLR4 antagonism, the *R. japonica* LPS might be a promising candidate scaffold for the development of antisepsis agents or as agents against inflammatory diseases. More broadly, this work supports the notion that marine Gram-negative bacteria harbor an unlimited reservoir of structurally unique LPS variants whose immunomodulatory properties remain largely untapped. Future studies will be essential to

deepen our understanding of the immunobiology of *R. japonica* KMM 9513^T LPS and to realize the translational potential of this marine LPS.

Experimental

Isolation and purification of the lipid A from *R. japonica* KMM 9513^T

R. japonica KMM 9513^T was sourced from the Collection of Marine Microorganisms at the G.B. Elyakov Pacific Institute of Bioorganic Chemistry (Far Eastern Branch, Russian Academy of Sciences). The strain was cultured for 48 hours at room temperature under aerobic conditions with agitation, using a liquid growth medium composed of (per liter): 5.0 g bacto peptone, 2.5 g yeast extract, 1.0 g glucose, 0.2 g K_2HPO_4, and 0.05 g $MgSO_4$, prepared in a mixture of 750 mL of natural seawater and 250 mL of distilled water.[11] Then bacterial cells were dried and extracted using the hot phenol/water procedure.[43,44] To eliminate traces of phenol and contaminants, the sample was subjected to prolonged dialysis against distilled water (Spectrum™, cut-off 12–14 kDa). To remove traces of nucleic acids and proteins, an enzymatic digestion was performed using DNase (Sigma-Aldrich, Darmstadt, Germany), RNase (Sigma-Aldrich, Darmstadt, Germany) and protease (Sigma-Aldrich, Darmstadt, Germany) followed by dialysis against distilled water (Spectrum™, cut-off 12–14 kDa). To assess the nature of the extracted sample, sodium dodecyl sulphate-poly-acrylamide gel electrophoresis (SDS-PAGE) was performed, followed by silver nitrate-gel staining. As additional steps of purification, ultracentrifugation (208 000×*g*, 4 °C for 18 hours) and washing with 500 μL of chloroform–methanol (1 : 2, vol/vol), followed by 500 μL of $CHCl_3/CH_3OH/H_2O$ (3 : 2 : 0.25, vol/vol/vol) and several steps of centrifugation (1200×*g*, 30 minutes) was also carried out. Finally, a repurification procedure, as previously described by Hirschfeld *et al.*,[45] was also performed to remove any possible traces of lipoprotein and/or lipopeptide contaminations. Then, an aliquot of the purified *R. japonica* LPS (30 mg) was subjected to mild acid hydrolysis in 100 mM sodium acetate buffer (pH 4.4) at 100 °C for 2 hours. Upon completion of the reaction, methanol and chloroform were added to the hydrolysate to achieve a ratio of CH_3OH/$CHCl_3$/hydrolysate 2 : 2 : 1.8 (v/v/v). The resulting mixture was vigorously mixed and centrifuged (4 °C, 8800×*g*, 20 minutes), and the lower chloroform phase was carefully recovered. Then, the organic layer was washed three times with a $CHCl_3/CH_3OH/H_2O$ mixture (2 : 2 : 1.8, v/v/v),[46] discarding the upper aqueous phase after each wash. Finally, the organic phase containing purified lipid A was dried under nitrogen flow and used for subsequent compositional and mass spectrometric analyses.

Chemical analyses

To investigate the fatty acid and monosaccharide composition of the lipid A moiety from *R. japonica* LPS, multiple chemical derivatization protocols were applied to purified LPS and isolated lipid A samples. For initial profiling, an aliquot of each sample was subjected to methanolysis using 1.25 M HCl in methanol at 85 °C for 16 hours. The resulting products were acetylated at 80 °C for 20 minutes to yield acetylated *O*-methyl glycosides (for sugar analysis) and methyl esters (for fatty acid analysis), which were subsequently analysed *via* GC-MS.[47,48] The monosaccharide profiling was used as a consistency check with our previously reported O-antigen structure.[11] In parallel, an identical methanolysis procedure was applied to isolated lipid A, followed by hexane extraction to isolate fatty acid methyl esters, which were also analyzed by GC–MS. Additional fatty acid profiling was performed by hydrolyzing lipid A with 4 M HCl at 100 °C for 4 hours, followed by alkaline treatment with 5 M NaOH at 100 °C for 30 minutes. The liberated fatty acids were extracted using chloroform after acidification (pH ∼ 3), methylated using diazomethane, and inspected *via* GC–MS. *O*-Linked fatty acids were specifically released by treating the samples with 0.5 M NaOH in CH_3OH/H_2O (1 : 1, v/v) at 85 °C for 2 hours. After acidification and chloroform extraction, the resulting fatty acids were methylated with diazomethane prior to GC–MS analysis. To determine the absolute configuration of 3-hydroxy fatty acids, samples were hydrolyzed with 4 M NaOH at 100 °C for 4 hours. The liberated 3-hydroxy acids were derivatized to form 3-methoxy acid L-phenylethylamide derivatives and subjected to GC–MS analysis. Retention times were compared to those of authentic standards.[49] All analyses were carried out on an Agilent 7820A gas chromatograph equipped with a 5977B mass selective detector and an HP-5 capillary column (30 m × 0.25 mm i.d.), using helium as a carrier gas at a flow rate of 1 mL min^{-1}.

MALDI-TOF MS and MS/MS analysis

MALDI-TOF MS and MS/MS spectra were acquired in resolution mode and negative ion polarity on a Waters SYNAPT XS mass spectrometer (Waters, Manchester, UK) equipped with an 8 kDa quadrupole and a MALDI source. The lipid A was dissolved in chloroform/methanol (50 : 50, vol : vol), while the matrix solution was formed by 2,4,6-trihydroxyacetophenone (THAP) (Sigma Aldrich) dissolved in methanol/0.1% trifluoroacetic acid/acetonitrile (7 : 2 : 1, vol : vol : vol) at a concentration of 75 mg mL^{-1}.[50] 0.5 μL of the sample and 0.5 μL of the matrix solution were applied on the MALDI plate and allowed to air dry at room temperature. Spots were randomly but evenly sampled, and experiments were executed in triplicate. Each MS/MS spectrum was generated using a trap collision energy ramp from 10 to 60 V. Red phosphorous was used to calibrate from 50 to 8000 Da. Nitrogen was supplied *via* a PLINIUS N45-1 nitrogen generator from CLAIND, and ultra-pure argon (SOL SpA) was used as collision gas in the trap cell. Data acquisition was performed using MassLynx™ v4.2 software, while the reported MS and MS/MS spectra were generated using Waters Connect software.

Reagents and cell lines

HEK-Blue™ hTLR4, HEK-Blue™ hTLR2 and THP1-Blue™ NF-κB cell lines were provided by InvivoGen (Toulouse, France). HEK-Blue™ cells were cultured in Dulbecco's Modified Eagle's

Medium (DMEM) supplemented with 10% heat-inactivated fetal bovine serum (FBS), 2 mM L-glutamine, 1% penicillin/streptomycin (Pen/Strep), and 100 μg ml^{-1} Normocin. To ensure plasmid selection, HEK Blue selection was added to the HEK-Blue™ cell culture medium. THP1-Blue™ NF-κB cells were cultured in the RPMI 1640 medium supplemented with 10% heat-inactivated FBS, 2 mM L-glutamine, 1% Pen/Strep, 25 mM HEPES and 100 μg ml^{-1} Normocin. Blasticidin was used to maintain plasmid selection in THP1 cells used according to the instructions of the manufacturer. All cell lines were grown at 37 °C in a humidified atmosphere containing 5% CO_2. Cell culture products including FBS, Pen/Strep, DMEM, RPMI 1640, glutamine, and HEPES were purchased from Thermo Fisher Scientific (Gibco), while phorbol 12-myristate 13-acetate (PMA) was obtained from Thermo Fisher Scientific (Kandel, Germany). In addition, Normocin, Blasticidin, HEK selection, *E. coli* O111:B4 LPS (*E. coli* LPS), *Rhodobacter sphaeroides* (RS) LPS (#tlrl-prslps), Quanti-Blue assay, PAM3CSK4 and anti-hTLR4 neutralization antibody (# mabg-htlr4-2) were obtained from InvivoGen (Toulouse, France).

LPS stimulation and Quanti-blue assay

HEK-Blue™ hTLR4 and HEK-Blue™ hTLR2 cells were seeded in a 96-well plate (3×10^4 per well). After allowing overnight attachment, HEK-Blue™ cells were stimulated for 18 hours with various concentrations (1–10–100 ng mL^{-1}) of *E. coli* LPS or *R. japonica* LPS. In addition, HEK-Blue™ hTLR2 cells were also treated with 500 ng mL^{-1} PAM3CSK4, which was used as a positive control of TLR2 activation. THP1-Blue™ NF-κB cells were seeded in a 96-well plate (60×10^3 cells per well) and differentiated following treatment with 5 ng mL^{-1} PMA for 24 hours and resting in a PMA-free medium for 72 hours.[51] The differentiated cells resulted in adhesion and were stimulated with different concentrations (1–10–100–1000 ng mL^{-1}) of *E. coli* LPS or *R. japonica* LPS for 6 and 24 h to perform immunological assays. HEK-Blue™ hTLR4, HEK-Blue™ hTLR2 and THP1-Blue™ NF-κB cell supernatants were collected to assess the secreted embryonic alkaline phosphatase (SEAP) levels using Quanti-Blue assay as an indicator of NF-κB activation following LPS stimulation, according to the manufacturer's protocol. The absorbance at 620 nm was detected using a TECAN Infinite M Plex spectrophotometer (Tecan, Grödig, Austria).

Competition assay

HEK-Blue™ hTLR4 and PMA-differentiated THP1 cells were primed with various concentrations of RS LPS or *R. japonica* LPS (0.1, 1, 10, and 100 ng mL^{-1} for HEK-Blue™ hTLR4 cells and 0.1, 1, 10, 100, and 1000 ng mL^{-1} for THP1 cells) for 4 hours and then stimulated with 10 ng mL^{-1} or 100 ng mL^{-1} of *E. coli* LPS (16 h for HEK-blue hTLR4; 24 h for THP1 cells).[52] THP1 cells were also pre-treated for 2 hours with *R. japonica* LPS (10–100 ng mL^{-1}) and, after the removal of supernatants, stimulated with *E. coli* LPS for 6 and 24 hours.

Cell viability (MTT) assay

Cell viability was assessed using a 3-(4,5-dimethylthiazol-2-yl)-2,5-diphenyltetrazolium bromide (MTT) assay. MTT was dissolved in PBS to obtain a 5 mg mL^{-1} stock solution and filtered through 0.22 μm filters. PMA-differentiated THP1 cells were treated with 200 μL of medium alone or containing various concentrations of *E. coli* LPS or *R. japonica* LPS for 24 hours in a 96-well plate. At the end of treatment, 20 μL of 5 mg mL^{-1} MTT stock solution was added to each well. After 3 hours of incubation at 37 °C, the medium was removed and the formazan crystals were dissolved with 200 μL of dimethyl sulfoxide (DMSO). Absorbance was measured on a TECAN Infinite M Plex spectrophotometer (Tecan, Grödig, Austria). Cell viability data were normalized towards unstimulated control cells.

Western blot

PMA-differentiated THP-1 cells were stimulated for 24 hours with the *E. coli* or *R. japonica* LPS and subsequently lysed in RIPA buffer (Thermo Fisher Scientific) supplemented with phosphatase and protease inhibitor cocktails (Thermo Fisher Scientific). Total protein content was quantified using a BCA Protein Assay Kit (Thermo Fisher Scientific). For western blot analysis, 30 μg of protein per sample was resolved on 4–20% Mini-PROTEAN® TGX Stain-Free™ Protein Gels (Bio-Rad) and transferred to nitrocellulose membranes using the Trans-Blot® Turbo™ Transfer System and 0.2 μm Mini Nitrocellulose Transfer Packs (Bio-Rad). The following primary antibodies were used: phospho-NF-κB p65 (Ser536) (1 : 500; #3033, Cell Signaling Technology), total NF-κB p65 (1 : 1000; #8242, CST), and GAPDH (1 : 3000; #97166, CST). HRP-conjugated secondary antibodies – anti-rabbit IgG (#7074, CST) and anti-mouse IgG (Cell Signaling Technology) – were used at a 1 : 2000 dilution. Immunoreactive bands were visualized using chemiluminescence and imaged with a ChemiDoc™ Imaging System (Bio-Rad).

Enzyme-linked immunosorbent assay (ELISA) assay

Cytokine levels were measured from THP1 supernatants upon *E. coli* or *R. japonica* LPS stimulation using a DuoSet ELISA kit (R&D system, Bio-Techne, Minneapolis, USA). Unstimulated cells were considered as a control for basal cytokine levels. Absorbance values were read at 450 nm with background subtraction at 570 nm using a TECAN Infinite M Plex spectrophotometer (Tecan, Grödig, Austria).

TLR4 blocking experiments

PMA-differentiated THP-1 cells were pretreated with 100 μL per well of 10 μg mL^{-1} of anti-hTLR4 neutralization antibody[53] for 2 hours and then stimulated with either *E. coli* or *R. japonica* LPS at different concentrations. Following 24 hours of stimulation, the Quanti-Blue assay was conducted as described above.

Statistical analysis

Data are shown as mean ± the standard deviation. Statistical analysis was assessed *via* an unpaired *t*-test using GraphPad

prism 10.0.1 software. A p-value <0.05 was considered statistically significant.

Conclusions

In conclusion, this work provides the first structural characterization of the lipid A moiety and a comprehensive immunological evaluation of the full LPS from the marine bacterium *R. japonica* KMM 9513^T. Mass spectrometry and chemical analyses revealed a highly heterogeneous lipid A profile, with unusual combinations of acyl chains and positional isomers that likely reflect adaptations to the dynamic conditions of marine ecosystems. Functionally, the purified LPS displayed low capacity to activate TLR4-mediated responses, while potently antagonizing pro-inflammatory signaling was triggered by *E. coli* LPS. At higher concentrations, residual NF-κB activity observed in TLR4-blocked macrophages suggested an additional involvement of alternative immune receptors, possibly linked to the unique features of the O-antigen portion. These findings support the possibility that the *R. japonica* KMM 9513^T LPS could inspire the design of synthetic analogs with tailored immunomodulatory properties and further emphasize the untapped immunological potential of marine bacterial glycoconjugates.[54]

Conflicts of interest

There are no conflicts to declare.

Data availability

The data supporting this article have been included as part of the ESI.†

Acknowledgements

F. D. L. acknowledges the European Research Council (ERC) under the Horizon Europe program under grant agreement no. 101039841 (DEBUGGING LPS). This work was also supported in part by the Italian Ministry of Foreign Affairs and International Cooperation (Italy–Germany Science and Technology cooperation – Call for joint research proposals for the years 2023–2025) to F. D. L. F. D. L. also acknowledges the Ministry of Education, Universities and Research, PRIN MUR 2022 (2022SHW3KY) and PRIN MUR PNRR 2022 (P202293ZMC). This research was also funded by the Russian Science Foundation (RSF), grant number 25-24-00401. *Rheinheimera japonica* KMM 9513^T was obtained from the Collective Facilities Center ''Collection of Marine Microorganisms (KMM) PIBOC FEB RAS'' of the G. B. Elyakov Pacific Institute of Bioorganic Chemistry, Far Eastern Branch of the Russian Academy of Sciences (Vladivostok, Russia).

References

1 N. I. Kalinovskaya, L. A. Romanenko and A. I. Kalinovsky, *Antonie van Leeuwenhoek*, 2017, **110**, 719–726.
2 B. Rekadwad, W. J. Li, J. M. Gonzalez, R. Punchappady Devasya, A. Ananthapadmanabha Bhagwath, R. Urana and K. Parwez, *3 Biotech*, 2023, **13**, 316.
3 M. Mercogliano, S. De Chiara, A. De Nicola, J. Cardellini, C. Montis, M. M. Yakimov, V. La Cono, F. Crisafi, A. Silipo, D. Berti, G. Milano, A. Molinaro and F. Di Lorenzo, *Chem. Sci.*, 2024, **15**, 17852–17861.
4 A. De Nicola, C. Montis, G. Donati, A. Molinaro, A. Silipo, A. Balestri, D. Berti, F. Di Lorenzo, Y. L. Zhu and G. Milano, *Nanoscale*, 2023, **15**, 8988–8995.
5 F. Di Lorenzo, K. A. Duda, R. Lanzetta, A. Silipo, C. De Castro and A. Molinaro, *Chem. Rev.*, 2022, **122**(20), 15767–15821.
6 F. Di Lorenzo, J.-M. Billod, S. Martín-Santamaría, A. Silipo and A. Molinaro, *Eur. J. Org. Chem.*, 2017, 4055–4073.
7 M. Ziaco, C. De Castro, A. Silipo, M. M. Corsaro, A. Molinaro, A. Iadonisi, R. Lanzetta, M. Parrilli and E. Bedini, *Carbohydr. Res.*, 2015, **403**, 182–191.
8 S. De Chiara, L. De Simone Carone, R. Cirella, E. Andretta, A. Silipo, A. Molinaro, M. Mercogliano and F. Di Lorenzo, *ChemMedChem*, 2025, **20**, e202400780.
9 P. Garcia-Vello, F. Di Lorenzo, D. Zucchetta, A. Zamyatina, C. De Castro and A. Molinaro, *Pharmacol. Ther.*, 2022, **230**, 107970.
10 F. Di Lorenzo, A. Silipo, R. Lanzetta, M. Parrilli and A. Molinaro, *Carbohydr. Chem.*, 2015, 57–89.
11 M. S. Kokoulin, A. I. Kalinovsky, S. V. Tomshich, L. A. Romanenko, V. V. Mikhailov and N. A. Komandrova, *Carbohydr. Res.*, 2016, **427**, 6–12.
12 B. Domon and C. E. Costello, *Glycoconj. J.*, 1988, **5**, 397–409.
13 F. Di Lorenzo, A. Palmigiano, S. Al Bitar-Nehme, L. Sturiale, K. A. Duda, D. Gully, R. Lanzetta, E. Giraud, D. Garozzo, M. L. Bernardini, A. Molinaro and A. Silipo, *Chem. – Eur. J.*, 2017, **23**, 3637–3647.
14 L. Zuliani-Alvarez, A. M. Piccinini and K. S. Midwood, *Bio Protoc.*, 2017, **7**, e2220.
15 W. Chanput, J. J. Mes and H. J. Wichers, *Int. Immunopharmacol.*, 2014, **23**, 37–45.
16 H. Schwende, E. Fitzke, P. Ambs and P. Dieter, *J. Leukoc. Biol.*, 1996, **59**, 555–561.
17 A. Tamby, J. S. Sinninghe Damsté and L. Villanueva, *Front. Mol. Biosci.*, 2023, **9**, 1058381.
18 E. Andretta, S. De Chiara, C. Pagliuca, R. Cirella, E. Scaglione, M. Di Rosario, M. S. Kokoulin, O. I. Nedashkovskaya, A. Silipo, P. Salvatore, A. Molinaro and F. Di Lorenzo, *Glycoconj. J.*, 2024, **41**, 119–131.
19 F. Di Lorenzo, *ALJMAO*, 2017, **110**, 1401–1412.
20 M. D. Pither, M. L. Sun, I. Speciale, A. Silipo, Y. Z. Zhang, A. Molinaro and F. Di Lorenzo, *Glycoconj. J.*, 2022, **39**, 565–578.
21 M. D. Pither, G. Mantova, E. Scaglione, C. Pagliuca, R. Colicchio, M. Vitiello, O. V. Chernikov, K. F. Hua, M. S. Kokoulin, A. Silipo, P. Salvatore, A. Molinaro and F. Di Lorenzo, *Microorganisms*, 2021, **9**, 2552.

22 R. Cirella, E. Andretta, L. D. S. Carone, F. Olmeo, M. L. Sun, M. Mercogliano and F. Di Lorenzo, *ChemBioChem*, 2025, e202500100.
23 N. Hassan, A. M. Anesio, M. Rafiq, J. Holtvoeth, I. Bull, A. Haleem, A. A. Shah and F. Hasan, *Front. Microbiol.*, 2020, **11**, 824.
24 T. J. Denich, L. A. Beaudette, H. Lee and J. T. Trevors, *J. Microbiol. Methods*, 2003, **52**, 149–182.
25 M. F. Siliakus, J. van der Oost and S. W. M. Kengen, *Extremophiles*, 2017, **21**, 651–670.
26 C. Buré, C. Le Sénéchal, L. Macias, C. Tokarski, S. Vilain and J. S. Brodbelt, *Anal. Chem.*, 2021, **93**, 4255–4262.
27 F. Di Lorenzo, C. De Castro, R. Lanzetta, M. Parrilli, A. Silipo and A. Molinaro, *Discovery Series*, RSC Publishing, 2015, pp. 38–72.
28 G. D. Kutuzova, R. M. Albrecht, C. M. Erickson and N. Qureshi, *J. Immunol.*, 2001, **167**, 482–489.
29 J. A. Holden, T. J. Attard, K. M. Laughton, A. Mansell, N. M. O'Brien-Simpson and E. C. Reynolds, *Infect. Immun.*, 2014, **82**, 4190–4203.
30 F. Di Lorenzo, A. Palmigiano, I. Paciello, M. Pallach, D. Garozzo, M. L. Bernardini, V. Cono, M. M. Yakimov, A. Molinaro and A. Silipo, *Mar. Drugs*, 2017, **15**, 201.
31 A. Ialenti, P. Di Meglio, G. Grassia, P. Maffia, M. Di Rosa, R. Lanzetta, A. Molinaro, A. Silipo, W. Grant and A. Ianaro, *Eur. J. Immunol.*, 2006, **36**, 354–360.
32 F. Di Lorenzo, A. Palmigiano, S. Albitar-Nehme, M. Pallach, M. Kokoulin, N. Komandrova, L. Romanenko, M. L. Bernardini, D. Garozzo, A. Molinaro and A. Silipo, *Eur. J. Org. Chem.*, 2018, 2707–2716.
33 S. I. Gringhuis, J. den Dunnen, M. Litjens, M. van der Vlist and T. B. Geijtenbeek, *Nat. Immunol.*, 2009, **10**, 1081–1088.
34 M. D. Pither, E. Andretta, G. Rocca, F. Balzarini, A. Matamoros-Recio, R. Colicchio, P. Salvatore, Y. van Kooyk, A. Silipo, F. Granucci, S. Martín-Santamaría, F. Chiodo, A. Molinaro and F. Di Lorenzo, *Angew. Chem., Int. Ed.*, 2024, **63**, e202401541.
35 S. M. Smith, *World J. Gastrointest. Pathophysiol.*, 2014, **5**, 133–146.
36 F. Nieto-Fabregat, Q. Zhu, C. Vivès, Y. Zhang, A. Marseglia, F. Chiodo, M. Thépaut, D. Rai, S. S. Kulkarni, F. Di Lorenzo, A. Molinaro, R. Marchetti, F. Fieschi, G. Xiao, B. Yu and A. Silipo, *JACS Au*, 2024, **4**, 697–712.
37 M. Maalej, R. E. Forgione, R. Marchetti, F. Bulteau, M. Thépaut, R. Lanzetta, C. Laguri, J. P. Simorre, F. Fieschi, A. Molinaro and A. Silipo, *ChemBioChem*, 2019, **20**, 1778–1782.
38 P. J. Brooks, Y. Wang, M. A. Magalhaes, M. Glogauer and C. A. McCulloch, *J. Cell Sci.*, 2020, **133**, jcs248864.
39 A. Zaal, R. J. E. Li, J. Lübbers, S. C. M. Bruijns, H. Kalay, Y. van Kooyk and S. J. van Vliet, *Front. Immunol.*, 2020, **11**, 305.
40 L. Zaffaroni and F. Peri, *Future Med. Chem.*, 2018, **10**, 461–476.
41 A. Romerio and F. Peri, *Front. Immunol.*, 2020, **11**, 1210.
42 Y. Xu, S. Chen, Y. Cao, P. Zhou, Z. Chen and K. Cheng, *Eur. J. Med. Chem.*, 2018, **154**, 253–266.
43 O. Westphal and K. Jann, *Methods Carbohydr. Chem.*, 1965, **5**, 83–91.
44 M. Tiemblo Martín, M. Coccimiglio, E. Andretta, L. De Simone Carone, A. Bell, T. Gerpe-Amor, C. Di Carluccio, A. Molinaro, Y. van Kooyk, N. Juge, F. Chiodo, F. Di Lorenzo and A. Silipo, *Carbohydr. Polym.*, 2025, **348**, 122833.
45 M. Hirschfeld, Y. Ma, J. H. Weis, S. N. Vogel and J. J. Weis, *J. Immunol.*, 2000, **165**, 618–622.
46 E. G. Bligh and W. J. Dyer, *Can. J. Biochem. Physiol.*, 1959, **37**, 911–917.
47 P. Garcia-Vello, I. Speciale, F. Di Lorenzo, A. Molinaro and C. De Castro, *Lipopolysaccharide Transport*, ed. P. Sperandeo, Humana, New York, 2022, vol. 2548, pp. 181–209.
48 M. Tiemblo-Martín, V. Pistorio, P. Saake, L. Mahdi, M. A. Campanero-Rhodes, R. Di Girolamo, C. Di Carluccio, R. Marchetti, A. Molinaro, D. Solís, A. Zuccaro and A. Silipo, *Carbohydr. Polym.*, 2024, **343**, 122433.
49 E. T. Rietschel, *Eur. J. Biochem.*, 1976, **64**, 423–428.
50 M. Pallach, F. Di Lorenzo, F. A. Facchini, D. Gully, E. Giraud, F. Peri, K. A. Duda, A. Molinaro and A. Silipo, *Int. J. Biol. Macromol.*, 2018, **119**, 1027–1035.
51 E. W. Baxter, A. E. Graham, N. A. Re, I. M. Carr, J. I. Robinson, S. L. Mackie and A. W. Morgan, *J. Immunol. Methods*, 2020, **478**, 112721.
52 F. Di Lorenzo, I. Paciello, L. L. Fazio, L. Albuquerque, L. Sturiale, M. S. da Costa, R. Lanzetta, M. Parrilli, D. Garozzo, M. L. Bernardini, D. A. Silipo and A. Molinaro, *ChemBioChem*, 2014, **15**, 2146–2155.
53 Z. Zhou, Y. Wu, L. Chen, L. Liu, H. Chen, Z. Li and C. Chen, *In Vitro Cell. Dev. Biol.: Anim.*, 2011, **47**, 541–549.
54 L. Fioretto, M. Ziaco, C. Gallo, G. Nuzzo, G. d'Ippolito, P. Lupetti, E. Paccagnini, M. Gentile, M. Della Greca, M. S. Appavou, L. Paduano, R. De Palma, A. Fontana and E. Manzo, *J. Colloid Interface Sci.*, 2022, **611**, 129–136.